QUARTERLY JOURNAL
OF THE
ROYAL METEOROLOGICAL SOCIETY

Vol. 122 APRIL 1996 Part A No. 531

Q. J. R. Meteorol. Soc. (1996), **122**, pp. 567–594

A vegetation–atmosphere interaction study for Amazonia deforestation using field data and a 'single column' model

By HUMBERTO R. da ROCHA[1]*, CARLOS A. NOBRE[1], JOSÉ P. BONATTI[1], IVAN R. WRIGHT[2] and PIERS J. SELLERS[3]

[1] *Centro de Previsão do Tempo e Estudos Climáticos–INPE, Brasil*
[2] *Institute of Hydrology, UK*
[3] *Goddard Space Flight Center–NASA, USA*

(Received 15 June 1994; revised 21 September 1995)

SUMMARY

The recent high deforestation rates in Amazonia have raised the question of how climate, mainly the precipitation patterns, might be affected as pasture land replaces the primary forest. This work initially shows how the dry season soil moisture and water stress in typical Amazonian pasture modifies the energy partitioning at the surface. Low-level moisture convergence is a primary mechanism to trigger convective cloud formation and precipitation. The relationship between moisture convergence and local surface evaporation in generating precipitation in Amazonia is studied utilizing a one-dimensional 'single column' model (SiB-1D). SiB-1D couples a surface-vegetation model (SiB) to a physical parametrization of deep convection (Kuo scheme), radiation, turbulent diffusion and large-scale precipitation. Model simulations for short periods (2 days) show its ability to calculate the Amazonian surface energy-balance components and boundary-layer dynamics when compared with field observations from the Rondônia Boundary-Layer Experiment and the Anglo-Brazilian Amazonian Climate Observation Study. The model was further used to test the sensitivity of the deep convection scheme to a range of typical low-level moisture convergence situations in a second experiment, and a third test investigated the local convective precipitation generated over forest and grass vegetation as a function of available soil moisture. Results showed that the rainfall over forest vegetation appeared to be almost insensitive to soil water stress whereas reduced precipitation was generated over pasture. When available soil water fell below a threshold of 60% the calculated precipitation over the pasture sites rapidly declined. Although these results are confined by the short integration period and the initial atmospheric profiles, they help to strengthen the notion that deforestation reduces evaporation and convective precipitation, especially during the dry season: a result already indicated by some previous general-circulation model experiments.

KEYWORDS: Amazon rain-forests Convection Deforestation Evapotranspiration Land-surface processes Vegetation

1. INTRODUCTION

The question has been raised concerning the role of tropical forests in controlling weather and climate, and whether the conversion of forest to pasture can affect large-scale precipitation patterns. Deforestation rates observed in the Amazonia region in the last two decades (Nobre *et al.* 1991) have consequently motivated field studies and modelling research to help answer these questions. Atmospheric moisture is obviously necessary for precipitation processes, and forests are an efficient moisture source to the planetary boundary layer (PBL) through evaporation, providing the conditions for moist convection to trigger cumulus growth and precipitation. It is believed that this role may be altered if short vegetation such as pasture replaces forest. However, statistical analysis of Amazonian

* Corresponding author, current affilliation: Universidade de São Paulo, DCA/IAG–Cidade Universitária, Rua do Matão, 1226, CEP: 05508-900, São Paulo, SP Brazil. e-mail: humberto@model.iag.usp.br.

rainfall data over a recent decade have not yet shown any trend in the time series of precipitation, see for example Rocha *et al.* (1989).

The influence of vegetation on hydrology can be investigated using a general-circulation model (GCM) in which parameters and surface variables are used to describe the vegetation–atmosphere interaction. The absorption of solar energy at the vegetated surface depends on canopy dimensions and vegetation-fraction cover. Surface temperature is a function of the amount of available energy absorbed at all wavelengths, and how it is partitioned into warming (sensible-heat flux) or moistening (latent-heat flux) the lower levels of the PBL. The interaction between soil type and vegetation is most important to hydrology, rainfall and runoff: soil type influences the rate of water extraction by the plants and, together with root depth, controls the ultimate volume available; vegetation generally enhances the infiltration of rainwater.

High and dense canopies can exert a significant drag force, reducing the surface wind speed and thus generating turbulence which enhances the evaporation of intercepted rainfall by single leaves, as well as diffusing water vapour through the mixed layer. Sensible-heat flux primarily forces growth of the mixed layer, whilst moisture from evapotranspiration is carried up through turbulent processes, providing humidity to trigger convective clouds above the PBL. While surface-energy partitioning and PBL dynamics act to provide moist static energy for cloud growth, solar energy is simultaneously blocked by clouds, leading to a negative feedback effect. As well as the adiabatic cooling taking place with the ascending motion within the clouds to produce precipitation, dynamical contributions can play an important role in these processes (Anthes 1984), particularly in areas where the mesoscale and synoptic-scale circulations largely determine the amount and location of precipitation. For this reason, to investigate the role of vegetation in convective processes, it is initially useful to study situations where the synoptic influence is weak.

Recent studies have shown that primary forests are not very sensitive to observed soil moisture deficits (Roberts *et al.* 1990). This is partially because forest root systems search for water deep into the soil during the dry season (Cerri and Volkof 1987). In contrast, grassland pastures in central Amazonia retain less solar energy (Bastable *et al.* 1993) and are very sensitive to soil moisture stress during dry spells (Wright *et al.* 1992); that is, evapotranspiration declines during the dry season.

Some analyses of changes in precipitation caused by land-cover change have been carried out by various numerical experiments, where a remarkable difference lies in the spacial domain of the models. Simulations by GCMs have been used to estimate the climatic effects of large-scale replacement of Amazonian tropical forests by grassy vegetation (e.g. Dickinson and Henderson-Sellers 1988; Lean and Warrilow 1989; Nobre *et al.* 1991). As reviewed by Salati and Nobre (1991), these studies were consistent in indicating that large-scale deforestation would lead to a warmer surface, consistent with a reduction in evapotranspiration: total precipitation would also decease. A different approach is to use mesoscale models to study the impact of surface inhomogeneities on smaller spatial scales, where the models are integrated for periods ranging from hours to a few days, for example Schadler (1990), showing the existence of ascending motion generated by contrasts in surface-energy balance comparable with sea-breeze motions. The studies of Pielke *et al.* (1991) have shown the importance of incorporating the contribution of mesoscale circulations to the vertical fluxes, a process not resolved in GCMs.

Within GCMs, dynamic equations control the atmospheric flow over resolutions compatible with a horizontal mesh in the order of 100 km, and it is expected that the GCM can represent the interaction of the large scale with smaller truncated scales. The so-called physical processes which are not explicitly resolvable are called the sub-grid processes, and have parametrizations that must represent their statistical effect on the grid cell. It has

been stated that their importance is significant for periods longer than one day, when they can represent sources or sinks of energy. Conversely, if a single model can represent satisfactorily all the physical processes interacting with each other on a short time-scale, one could understand how isolated parametrizations are sensitive to the simulated variability in the others, bearing in mind that the large-scale effects, i.e. the horizontal components, are absent or weak. Therefore, the main purpose for building a one-dimensional (1-D) vertical model of the atmosphere is to deal with the most important physical parametrizations represented in the column. For example, Rabin *et al.* (1990) used a 1-D model approach to show how soil moisture influences the onset of convective cloud growth.

This work addresses the prediction of surface-energy partitioning over typical central Amazonia ranch land, and its clear dependence on soil water deficits. The Simple Biosphere Model (SiB) (Sellers *et al.* 1986) is calibrated for two Anglo–Brazilian Amazonian Climate Observation Study (ABRACOS) pasture sites (Manaus and Ji-Paraná), and the calibrated parameters are used to validate a 1-D single-column atmospheric model (hereafter referred to as SiB–1D). The model was built as an adaptation of the Center for Ocean–Land–Atmosphere studies (COLA) SiB–GCM to represent the atmospheric physical processes (Sato *et al.* 1989). SiB-1D was initialized with observed sounding profiles of the PBL, and integrations were performed assuming the absence of large-scale interactions. Calculations of the surface and boundary-layer variables are compared with data collected by the ABRACOS and the Rondônia Boundary-Layer Experiment (RBLE). An assessment of the precipitation parametrization is discussed to understand the sensitivity of the model to evaporation and the external forcing of PBL moisture convergence, where the mean diurnal cycle of observed precipitation is compared with model calculations. The results of the SiB-1D integrations form a basis for discussing how the surface vegetation (forest or pasture) influences the simulated precipitation, taking account of the soil moisture dependence.

2. Energy partition and soil moisture availability at Fazenda Dimona

Figure 1 shows field measurements of energy fluxes, soil moisture and rainfall recorded at Fazenda Dimona, a cattle ranch about 100 km north of Manaus (02°19′S, 60°19′W) with pasture vegetation. Data were collected during the first two intensive field missions of the ABRACOS which extended from 16 September 1990 to 2 November 1990 and from 30 July 1991 to 10 September 1991 (hereafter referred to as M1 and M2 respectively) (see the appendix for detailed data description). Although the two blocks of data (M1 and M2) shown in Fig. 1 do not cover a continuous seasonal cycle, and there is an unusually prolonged dry season during M1, observational evidence (*Climanálise*, vol. 5, no. 8, pp. 1–3) suggests that the early dry season in 1990 (before September) was not anomalous, and is therefore comparable with the M2 data concerning the vegetation status. Thus they provide a good example of the micrometeorological and climatological behaviour of the Manaus pasture site during the early (M2) and the late (M1) parts of the central Amazonia dry season (July to October). Taking M1 and M2, chronologically reversed, as a single near-continuous data period, the daily rainfall over the site diminished (Fig. 1(d)), while the net radiation showed a slight positive trend (Fig. 1(a)), indicating an overall decrease in cloud cover during the dry season. A change of 21% in the soil moisture (425 to 350 mm) through this period was observed. Although the clay soil has high permeability and porosity, the maximum available water content is not large, producing the decrease of water availability from 100% (field capacity) to about 55% at the end of the M1 dry season (Fig. 1(c)). When available moisture is reduced to half, extreme soil suction makes it difficult for the shallow-pasture root system to extract further water.

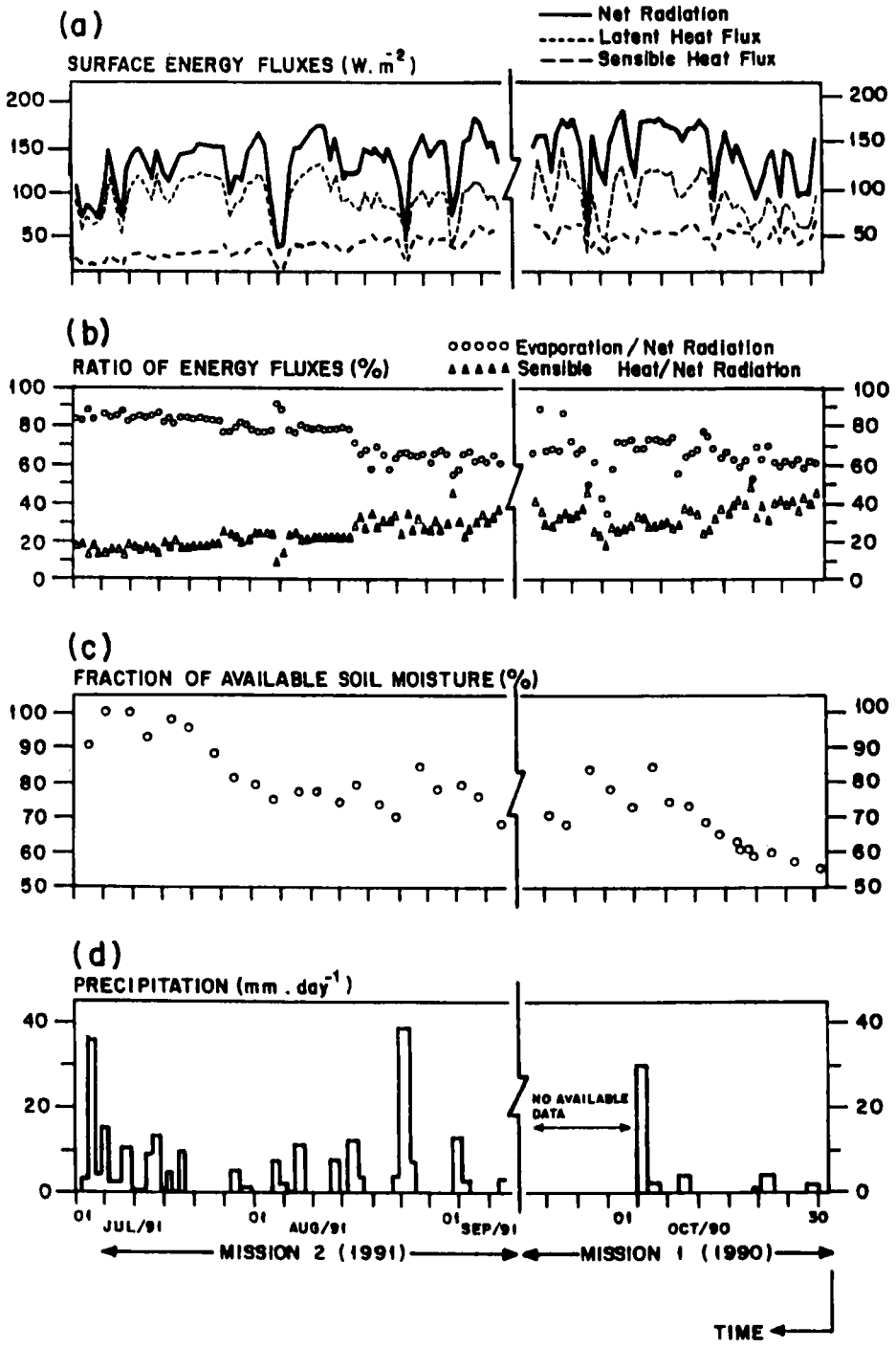

Figure 1. Micrometeorological and hydrological data collected during the ABRACOS field campaigns for the grass site of Fazenda Dimona, Manaus, during early to mid dry season (mission 2—30 July to 10 September 1991) and mid to late dry season (mission 1—16 September to 2 November 1990): (a) surface energy fluxes, (b) ratio of surface energy fluxes, (c) fraction of available soil moisture in the top metre; and (d) precipitation.

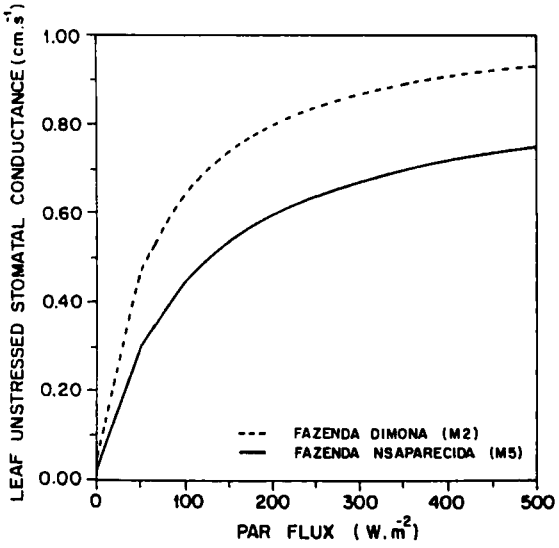

Figure 2. Leaf unstressed stomatal conductance as a function of photosynthetically active radiation (PAR) flux calculated using the calibrated light dependent stomatal response parameters for Fazenda Dimona for mission 2 and Fazenda NSA for mission 5.

The direct consequence of this water stress is a distinct trend in the time series of energy partitioning: the fraction of available energy used for evapotranspiration decreased from approximately 85% to around 60% (Fig. 1(b)). Wright *et al.* (1995) showed that vegetation was significantly more stressed by soil moisture in M1 than in M2.

3. SiB CALIBRATION

The SiB–1D atmospheric model was run separately for two different Amazonian pasture sites using the parameters specific to each site, including the seasonal (structural) parameters associated with the initialization and validation data. The sites were Fazenda Dimona (M2, see section 2), and Fazenda Nossa Senhora da Aparecida (10°47′S, 62°22′W, hereafter referred to as Fazenda NSA), using the data of the 5th intensive mission of the ABRACOS (hereafter referred to as M5) which took place in Ji-Paraná during July 1993. A complete description of the data set and optimization procedures are described in the appendix.

An important distinction between the two sites is that the Bowen ratio during M5 was substantially higher than that of M2, being partly due to differences in soil moisture availability and partly a result of the vegetation status during the different dry season periods. The region of Ji-Paraná is located in south-western Amazonia, which is often influenced by the penetration of extratropical cold-weather systems during wintertime, causing temperatures as low as 10 °C in this region. Local farmers have noticed that the pastures are very sensitive to these cold periods, which usually last a few days. The pasture can become still drier if the penetration of these cold fronts is concurrent with the winter dry season. A contrast in the modelled response of the two vegetation types can be seen in Fig. 2, which compares the optimized functions for leaf unstressed stomatal conductance for photosynthetically active radiation (PAR) (parameters a, b and c, see the appendix) for M2 and M5, wherein the Fazenda Dimona response (M2) suggests a more efficient use of visible radiation for transpiration than at Fazenda NSA (M5). However, it is

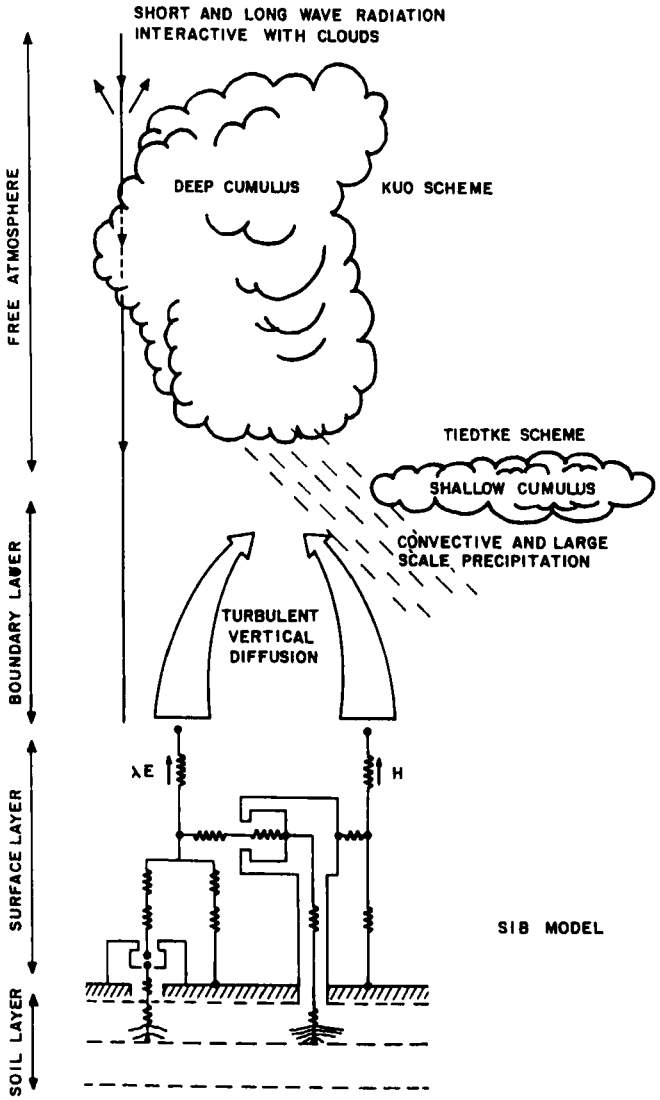

Figure 3. Pictorial representation of the physical processes parametrized in the SiB-1D model (see text): surface (SiB model), vertical turbulent diffusion in the boundary layer, shallow and deep cumulus convection, short- and long-wave radiation interactive with deep convection, and large-scale precipitation. (λE is evaporation and H is sensible heat).

acknowledged that this difference may be partly due to the interdependence of parameters in the multivariate optimization procedure.

4. The SiB-1D model

(*a*) *Description*

This paper describes a one-dimensional single-column model (SiB-1D) developed to couple the SiB model to physical parametrizations of the atmosphere, based on the COLA GCM (Fig. 3). The processes described in SiB-1D are as follows: (i) the SiB model, as described by Sellers *et al.* (1986) and Sato *et al.* (1989), incorporating modifications in the

aerodynamic transfer of Xue *et al.* (1991); (ii) closure order 2.0 turbulent vertical diffusion of Mellor and Yamada (1982); (iii) vertical flux divergence and radiative heating (cooling) described by the short-wave radiation-transfer scheme of Lacis and Hansen (1974), as modified by Davies (1982); the long-wave radiation-transfer scheme proposed by Harshvardhan and Corsetti (1984) including the efficient-radiation scheme of Harshvardhan *et al.* (1987) to permit the simulation of the diurnal cycle; and the scheme of radiation interaction with cloud cover developed by Slingo (1987); (iv) the shallow cumulus convection scheme of Tiedtke (1984); a deep cumulus convection scheme of Kuo (1974) as modified by Anthes (1977) and Philips (1979), and a large-scale precipitation parametrization to take account of supersaturation effects. The model is hydrostatic and is therefore insensitive to subsidence effects. A further simplification of the scheme of Slingo (1987) assumes that the vertical velocity is zero.

The prognostic variables are calculated in the atmospheric column with a vertical structure having 40 layers (sigma p coordinates, equal to the pressure at a level upon the surface pressure), namely the potential temperature, θ, and the air specific humidity, q. Temporal rates of these variables are given by

$$\frac{\partial \theta}{\partial t} = -\frac{\partial}{\partial z}(Q_H) - \frac{1}{\rho}\frac{\partial}{\partial z}\left(\rho K_T \frac{\partial \theta}{\partial z}\right) + \frac{\lambda}{c_p}\left(\frac{\bar{C}}{\pi} + \delta \bar{C}_{LS}\right) - \frac{1}{\rho c_p}\frac{\partial Q}{\partial z} \qquad (1)$$

(i) (ii) (iii) (iv) (v)

$$\frac{\partial q}{\partial t} = -\frac{\partial}{\partial z}(Q_E) - \frac{1}{\rho}\frac{\partial}{\partial z}\left(\rho K_Q \frac{\partial q}{\partial z}\right) - (\bar{C} + \delta \bar{C}_{LS}) \qquad (2)$$

(i) (ii) (iii) (iv)

where (i) is the divergence of turbulent vertical fluxes of heat ($Q_H = \overline{w'\theta'}$) or humidity ($Q_E = \overline{w'q'}$) in the boundary layer, where the primed quantities denote the effects of the sub-grid scale on the grid scale (bar quantities); (ii) is the heat or humidity profile adjustment by shallow convection; (iii) is the temperature or humidity convective adjustment resulting from the condensational heating by deep convection, $\bar{C}$, where π is the Exner function; (iv) is the effect of large-scale precipitation in a supersaturated profile, in which adjustment is approximated by the wet-bulb process; and (v) is the diabatic heating by the divergence of the short- and long-wave radiative fluxes, Q, in the column.

All the simulations described hereafter are of 52-hours duration, with a 20-minute time step starting at 00 UTC. The 52 hours comprise 48 hours, local midnight to midnight, plus four hours from the initialization hour of 00 UTC (2000 h local time). The model is initialized with an atmospheric profile of temperature, humidity, meridional and zonal wind, which are sigma-coordinated interpolations from a radiosonde profile. The geographic position and time are specified to initialize the radiation sub-model. The surface pressure is held constant. Wind speed values are provided for each time step by interpolating in time between observed radiosonde profiles. Short-wave radiation is calculated every hour and linearly interpolated for the smaller time interval. The long-wave radiation routines update the atmospheric cooling rates every 3 hours.

(*b*) *Initialization data for SiB-1D simulations*

Data to describe the initial structure of the PBL were taken from sounding experiments, using radiosondes, and a tethered balloon, conducted over forest and pasture near Ji-Paraná, Rondônia, and over the forest near Manaus, Amazonas. Data representing the Ji-Paraná area of Brazil were collected during the second field campaign of the RBLE (RBLE-II). The forest site was at Reserva Biológica do Jarú, 10°05′S, 61°56′W, (hereafter

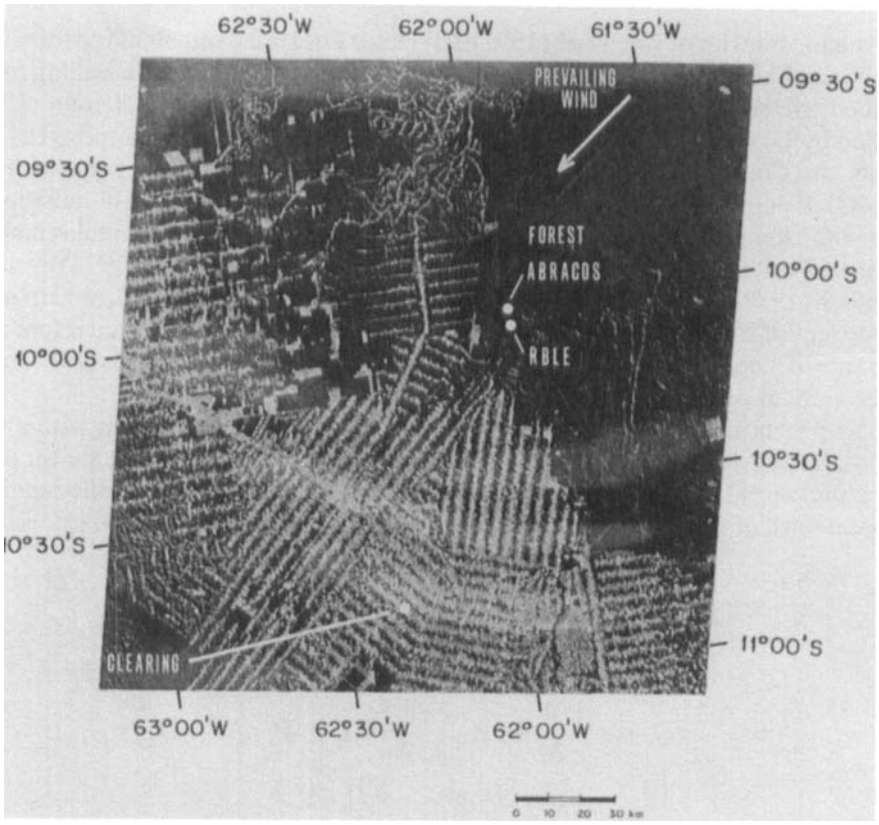

Figure 4. Landsat satellite image (1991) showing the forested and cleared areas in the region of Ji-Paraná, Rondônia, south-western Amazonia. The location of the ABRACOS and RBLE sites over forest and grass are indicated.

referred to as Reserva Jarú), which is administrated by the Instituto Brasileiro do Meio Ambiente e Recursos Naturais Renováveis (IBAMA). For logistical reasons, the tethersounding and radiosounding instruments were operated from a small clearing (10°09′S, 61°54′W) about 7 km from the forest micrometeorological tower on which the turbulent fluxes were measured. PBL measurements consisted of radiosonde profiles and boundary-layer tethersounding of temperature, humidity and wind speed and direction, and were recorded every 3 hours throughout the day and night, commencing at 2000 h local time. Both forest and pasture sites were collocated with the ABRACOS field-measurement sites in Rondônia, and coincident with the M5 surface turbulent flux measurements. Boundary-layer measurements were made over the forest from 3 to 12 July 1993. The pasture-site measurements were recorded at Fazenda NSA (see site description in section 3(a)) from 17 to 26 July 1993. The study area within Rondônia is shown by satellite image in Fig. 4. Upper-air and boundary-layer data from Manaus were collected at the Reserva Ducke forest (02°57′S, 59°57′W) during the field experimental campaign of the Amazon Boundary Layer Experiments, ABLE-2A, within the dry season months of July and August of 1985 (see Martin *et al.* 1988). Micrometeorological data are those collected during the Amazon Region Micrometeorological Experiment (ARME) described by Shuttleworth (1988).

Table 1 shows the initial and boundary conditions for the SiB-1D numerical experiments further described in sections 4(c), 4(d) and 4(e). Cases c1 and c2 are discussed in section 4(c), where model calculations are compared with observations. Cases d1 and d2

TABLE 1. INITIAL AND BOUNDARY CONDITIONS FOR THE SIMULATIONS WITH THE SiB-1D MODEL DESCRIBED IN SECTIONS 4(c) (c1 AND c2), 4(d) (d1 AND d2) AND 4(e) (e1 TO e3)

Case	Surface vegetation type	Calibration site for SiB parameters	Initial date	Content of initial precipitable water (mm)	Variation of soil moisture	β parameter of Kuo scheme (%)
c1	Forest	RDucke	4 July	43	—	47
c2	Grass	FNSA	24 July	28	—	62
d1	Forest	RDucke	4 July	43	—	47
d2	Grass	FNSA	24 July	28	—	62
e1	Forest	RDucke	31 July	52	Yes	25
e2	Grass	FNSA	31 July	52	Yes	25
e3	Grass	FDimona	31 July	52	Yes	25

All simulations start at 00 UTC for a period of 52 hours.

* R Ducke—Reserva Ducke; FDimona—Fazenda Dimona; FNSA—Fazenda Nossa Senhora Aparecida.

refer to the investigation of model sensitivity to a range of external forcings of the PBL moisture convergence, described in section 4(d). Cases e1 to e3 are discussed in section 4(e), where changes in the convective and large-scale precipitation results are investigated in response to a range of soil moisture conditions under both forest and grass vegetation in Amazonia.

(c) *Comparison of the SiB-1D data with the RBLE-II and ABRACOS data*

The performance of the SiB-1D model and its ability to simulate the surface and boundary-layer variables when compared with observations are now discussed. The model is integrated for two cases (c1 and c2, see Table 1). The c1 case is initialized with a profile measured over Reserva Jarú at 00 UTC 4 July 1993. The parameters for the SiB model to represent the forest vegetation were taken from the tropical forest biome given by Sellers *et al.* (1989). The c2 case refers to an initialization using the profile collected at the grass site of Fazenda NSA at 00 UTC 24 July 1993. The SiB parameters for pasture vegetation were those calibrated for M5 (see section 3(b)).

Figure 5 shows the time evolution of the virtual potential temperature in the boundary layer for cases c1 (forest—4 and 5 July 1993) and c2 (grass—24 and 25 July 1993). The representation of the nocturnal boundary layer by stratified layers near the lower levels of the atmosphere can be seen in the first hours of the simulation, and is a consequence of the initial conditions. In the transition from the first to the second day of simulation, the nocturnal stratification develops from about 1800 h local time (dusk), and continues until dawn. Above the stratified depths a residual mixing layer persists during the night. The mixed layer during the daytime is represented by the near-neutral profiles which are limited by the temperature inversion at the top of the mixed layer.

A comparison of the calculated PBL virtual potential-temperature profile with observations is shown in Fig. 6 for the forest site (c1). The well-mixed-layer profile at 1700 h local time is shown in Figs. 6(a) and 6(c) for 4 and 5 July 1993, respectively, and the nocturnal boundary layer is shown in Fig. 6(b) for 0500 h local time on 5 July 1993. A reasonable agreement is obtained, with a small discrepancy in the exact level where the mixed-layer inversion occurs: the observed level on 4 July was about 1300 m, while the calculated profile shows this transition at 1100 m. The temperature inversion observed in the nocturnal boundary layer is well represented at about 300 m for both calculations and

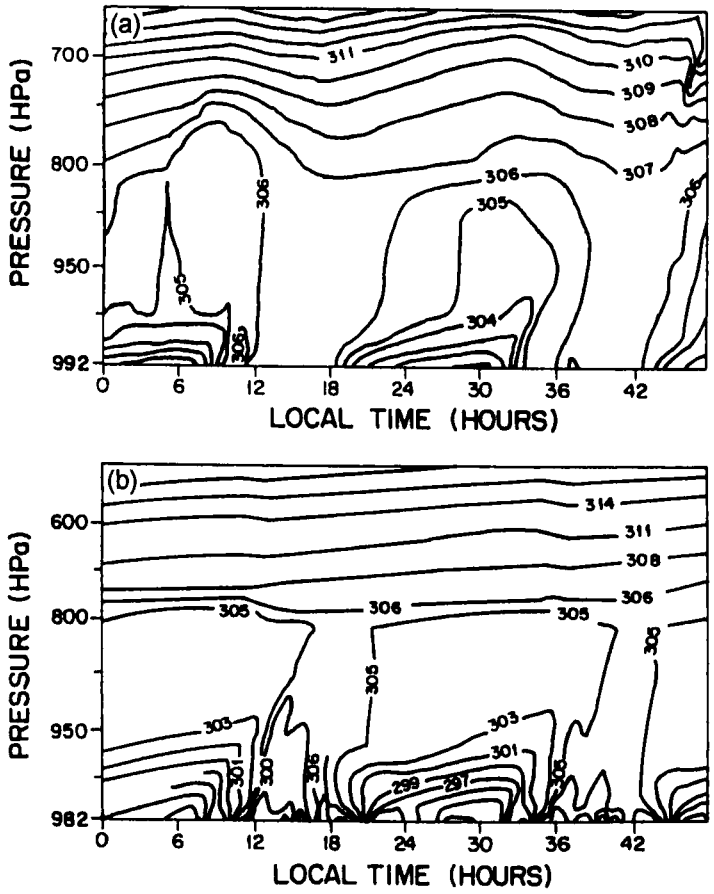

Figure 5. Virtual potential temperature (K) in the low troposphere calculated by the SiB-1D model for (a) case c1 (forest, 4–5 July 1993) and (b) case c2 (grass, 24–25 July 1993).

observations. The residual mixed layer just above the stratified layer is also reasonably represented by the calculated profile, although this calculated value is approximately 1.5 K cooler than observations of maximum inversion height at about 800 m.

Cloudiness, which attenuates solar radiation, is a factor which greatly controls surface temperature. Figure 7 shows the condensational heating resulting from deep convection, and the heating and cooling associated with turbulent transfer parametrized by the shallow cumulus convection. Figure 6(d) shows the calculated and observed surface temperatures over the forest site (c1) with satisfactory agreement except for between 1000 h local time and noon. These differences are a consequence of the discrepancy in the incoming solar radiation, as shown in Fig. 6(e), created by the difference in timing in the onset of cloud development. For the forest site, model calculations of deep convection start at about 0900 h local time (Fig. 7(a)) and the calculated net radiation and the turbulent fluxes (Figs. 6(f), 6(g) and 6(h)) followed the diurnal pattern imposed by solar radiation.

A first point to discuss is that the model layers are cloud-free until the mechanism of convection begins. Only after convective clouds are generated can the radiation scheme 'detect' them and reflect back short wave to the upper atmosphere. This effect can be seen for the calculated solar radiation in Fig. 6(e), where there is a sharp decline in insolation after a peak value of about 900 W m^{-2}; also the calculated maximum solar radiation is out

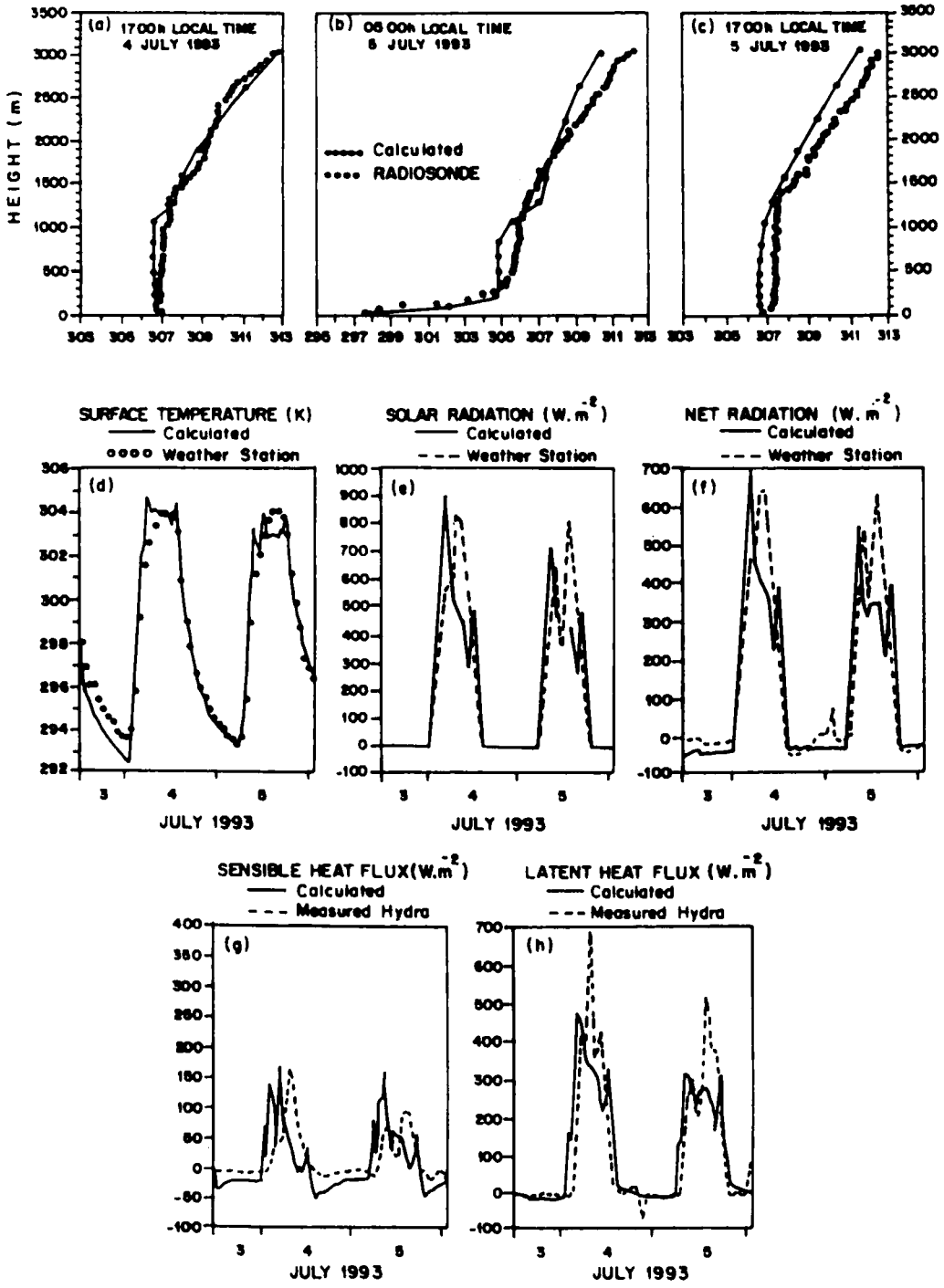

Figure 6. Surface and boundary-layer variables for case c1 (forest, 4–5 July 1993) calculated by the SiB-1D model and observed. Atmospheric profile of virtual potential temperature (K): (a) 1700 h local time on 4 July, (b) 0500 h local time on 5 July, and (c) 1700 h local time on 5 July; (d) surface temperature; (e) total solar radiation; (f) net radiation; (g) sensible-heat flux, and (h) latent-heat flux.

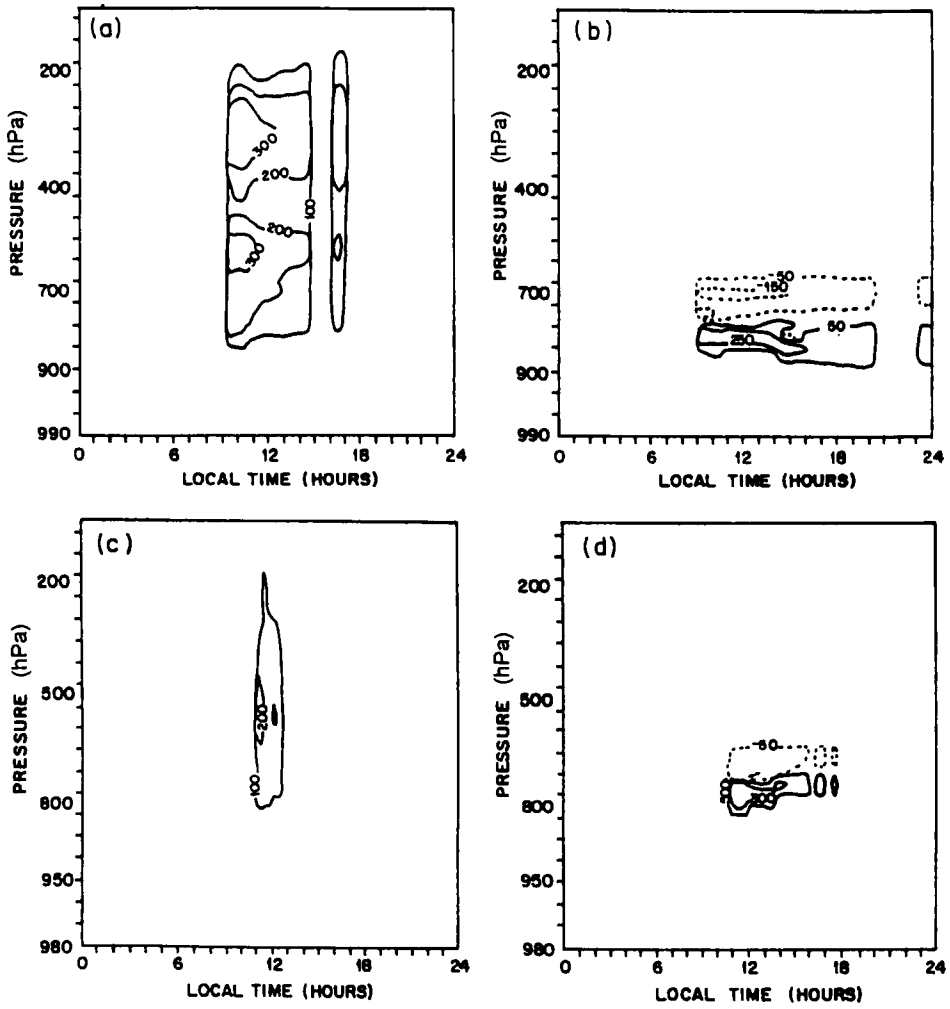

Figure 7. Condensational heating calculated by the SiB-1D model for (a) case c1 (forest, 4 July 1993) and (c) case c2 (grass, 24 July 1993); calculated temporal rate of temperature in the shallow cumulus parametrization for (b) case c1 (forest, 4 July 1993) and (d) case c2 (grass, 24 July 1993). Units in 10^{-3}k h^{-1} with negative values shown dashed.

of phase with the observations. The observed insolation is smoothly attenuated during the course of the day, mostly as a result of shallow cumulus. Also, as the short-wave scheme only takes account of column transmissivity each hour, the model cloud generation may lag by up to one hour behind the calculated convective precipitation. The absence of modelled night-time convective clouds is consistent with observations, resulting in a good agreement of observed and calculated surface temperatures in the night from 4 to 5 July 1993.

Secondly, the calculated atmospheric transmissivity is based on climatological concentration of ozone and carbon dioxide, and the updated amount of water vapour. Although measurements of atmospheric transmissivity were not taken during M5, smoke and aerosol loading from regional burning are common during the dry season (Pereira and Setzer 1989) and can contribute to increased atmospheric albedo and decreased insolation.

The model calculated a total precipitation of about 4 mm for the case c1 simulation. The absence of observed precipitation is likely to be a result of synoptic-scale subsidence

TABLE 2. TWO-DAY AVERAGE DAYTIME VALUES OF THE SURFACE ENERGY-BALANCE COMPONENTS FROM SIMULATIONS FOR THE FOREST (CASE c1) AND GRASS SITE (CASE c2) AND THE CORRESPONDING FIELD OBSERVATIONS

	Forest		Grass	
	case c1	observed	case c2	observed
	$W\ m^{-2}$			
Insolation (S)	203	230	266	239
Net radiation (R_n)	154	156	162	141
Evaporation (λE)	120	120	80	75
Sensible heat (H)	23	23	53	66
Soil heat flux (G)	6	1	16	10
Residual ($R_n - \lambda E - H - G$)	5	12	12	−10

inhibiting cloud formation, a factor not accounted for in the 1-D model simulation. The first and second columns of Table 2 show the observed and simulated two-day averages of daytime surface-energy-balance components. For the first case (c1), despite the diurnal differences in the observed and simulated insolation, the daily values of net radiation and energy partitioning between sensible- and latent-heat flux agree well with the observations on a daily basis.

The simulation for the grass site (c2) is illustrated in Fig. 8 and shows the calculated and observed surface variables for 24 and 25 July 1993. The calculated daytime mixing-layer depth at 1700 h local time on 24 July (Fig. 8(a)) agrees well with observations at a height of about 1800 m, but a small difference of 0.5 K is noticed throughout the mixed layer. The calculations at 1700 h local time on 25 July, 24 hours later (Fig. 8(c)), do not agree as well as on the first day: calculated PBL virtual potential temperature is about 1.5 K cooler and the PBL height is 1700 m compared with the observed 2100 m.

The calculated condensational heating by deep cumulus and the reduced heating/cooling by shallow cumulus convection over the grass site (c2, Figs. 7(b) and 7(d), respectively) are of shorter durations than those calculated over the forest (c1, Figs. 7(a) and 7(c)). The calculated convection also began later and ended earlier over the grass as compared with the forest. This is partly due to the lower evaporation rates from the grass site which reduces the input of water vapour into the PBL. A direct consequence of this low cloud-cover fraction is that the solar radiation reached a peak of about 1000 $W\ m^{-2}$ and caused the surface temperature to reach much larger values than observed (Fig. 8(d)). The surface variables shown in Fig. 8 for case c2 were derived from a simulation which was initialized with a cloud-free column and, as previously mentioned, the onset of cloudiness is due to the mechanism of deep convection.

It is also important to consider the forcing by advective terms with respect to the local measurements. Synoptic-scale weather systems over the region during the period 24–25 July caused large-scale subsidence and decreased the values of precipitable water down to 23 mm. Stronger than usual daytime winds in the PBL, ranging from 5 to 10 $m\ s^{-1}$, were also noticed. This suggests the possibility of a significant contribution from turbulent eddies, resulting from mesoscale circulations and leading to a mechanical forcing of the mixing layer. If synoptic-scale or mesoscale factors partly helped to force PBL growth in this period, the conditions for 1-D model simulations may not be fully valid, thus leading to discrepancies in the calculated values.

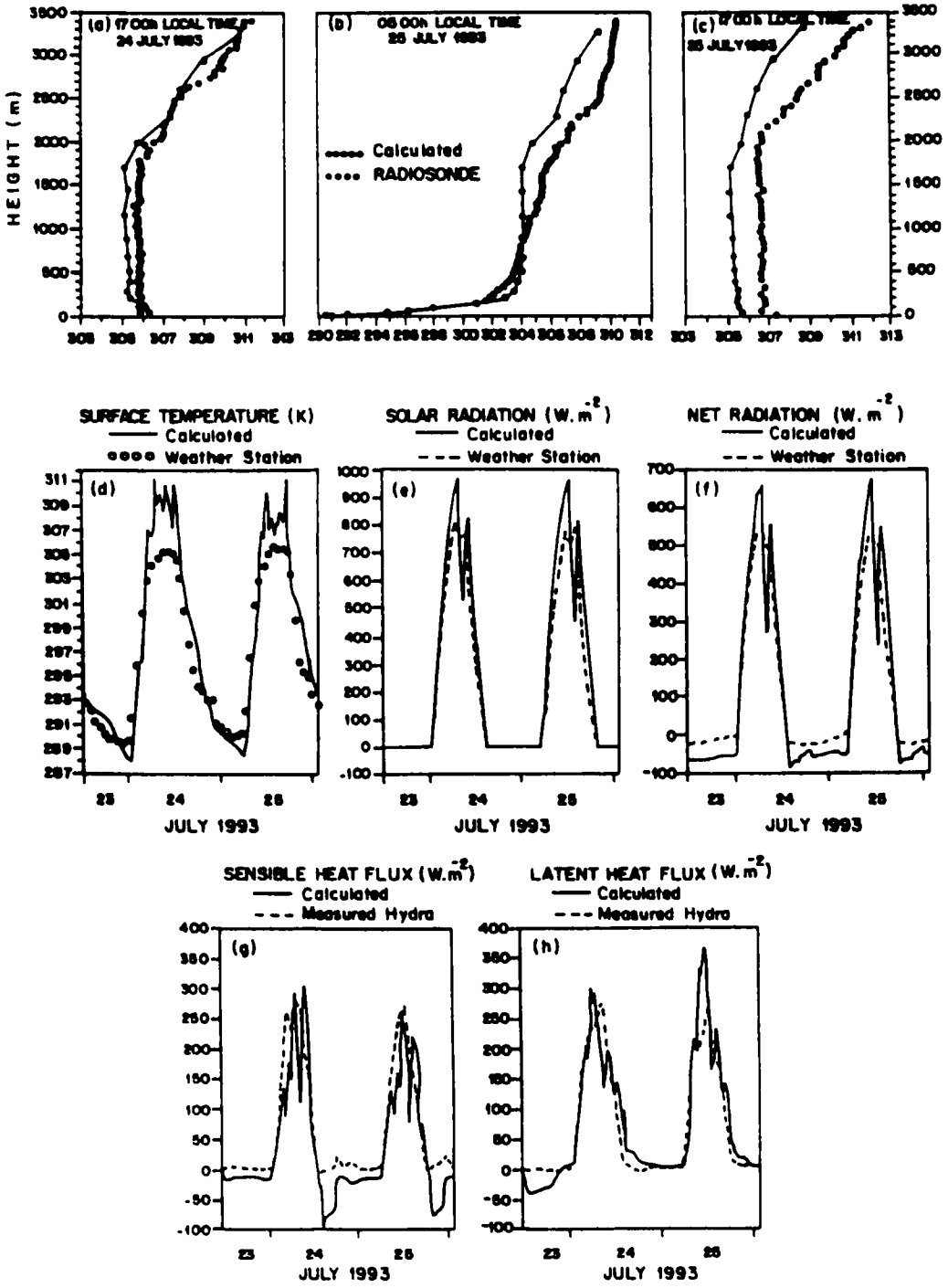

Figure 8. Surface and boundary-layer variables for case c2 (grass, 24–25 July 1993) calculated by the SiB-1D model and observed. Atmospheric profile of virtual potential temperature (K): (a) 1700 h local time on 24 July, (b) 0500 h local time on 25 July, and (c) 1700 h local time on 25 July; (d) surface temperature; (e) total solar radiation; (f) net radiation; (g) sensible-heat flux, and (h) latent-heat flux.

(*d*) *Sensitivity of calculated precipitation to PBL moisture convergence forcing*

The Kuo scheme for deep cumulus convection has the low-level moisture convergence as the principal mechanism for maintaining convection. It has inherent limitations of scale when used in 3-D models. In the SiB-1D model, the scheme is expected to represent the interaction of convection with other physical processes over an average horizontal area of flat terrain wherein the mesoscale effects are integrated: generating precipitation and thus condensational heating, reflecting short-wave, absorbing/emitting long-wave radiation, and so adjusting the profiles of temperature and humidity. The moisture increase in the column, M_t, is proportional to the vertically integrated temporal rate of moisture convergence, originating from advection, Q_a, and/or surface evaporation, Q_e, as follows:

$$M_t = -\frac{1}{g}\int_0^{p_s} (Q_a + Q_e)\, dp. \tag{3}$$

The condensed water vapour is precipitated out, while the remaining portion increases the specific humidity of the column, q: a process regulated by the β parameter. β is the fraction of the total water vapour convergence used to increase the humidity of the column, while $(1 - \beta)$ is condensed and precipitated. A linear approach is employed here, given by

$$\beta = 1 - \frac{\langle q \rangle}{\langle q_s \rangle} \tag{4}$$

where $\langle\ \rangle$ refers to the vertical column average. While in section 4(c) the term Q_a was zero (only evaporation was a source for convection), here a source of moisture is imposed on the lower levels of the PBL in order to represent the role of large-scale moisture convergence. This method is based on a similar forcing to that of Silva Dias *et al.* (1987), which is sinusoidal in time and is maximum for the lowest layer, decreasing to a minimum pressure layer set at 770 hPa, it is written as:

$$Q_a = (Q_{max}) \cos\left(\frac{2\pi t}{24}\right) \cos\left(\frac{2\pi p}{p_s}\right). \tag{5}$$

To investigate how the Kuo scheme responds to external forcing, within the SiB-1D model, water vapour was 'pumped' artificially into the column. Daytime forcing was active from 0600 to 1800 h local time with Q_{max} varying from 2 to 20 mm day^{-1}. Two cases were set for the boundary and initial conditions (see Table 1): the first, d1, was initialized assuming forest vegetation with an initial profile collected over Reserva Jarú at 00 UTC 4 July 1993; the second, d2, was initialized using data collected over Fazenda NSA at 00 UTC 24 July 1993. The profiles contained very different amounts of precipitable water: 43 mm and 28 mm over the forest and grass sites, respectively.

The simulation over the forest site (Fig. 9(a)) showed a convective precipitation intensity and duration increasing with the daily amount of forced convergence. Evaporation, in the absence of external forcing, was able to produce a maximum precipitation of 0.3 mm h^{-1}, while a forcing of 20 mm day^{-1} increased this to about 1.2 mm h^{-1}. Input moisture which did not precipitate was used to moisten the column: in the second day of simulation, the moisture convergence was sufficient to produce higher precipitation peaks compared with the first day.

For the grass simulations (Fig. 9(b)), a similar behaviour to that of the forest was indicated, in which larger amounts of moisture input produced higher precipitation intensities. The wetting up of the column after the first day, as in Fig. 9(a), produces larger precipitation peaks in the second day. It should be pointed out that the calculated precipitation is different in magnitude between the forest and the grass cases, the latter being

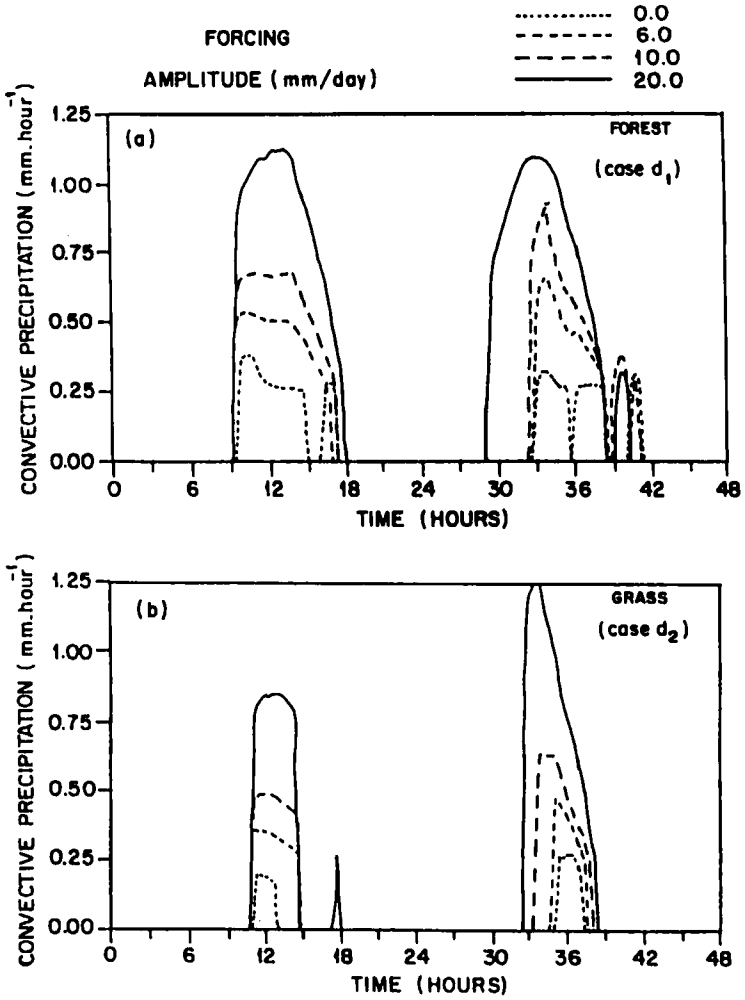

Figure 9. Calculated convective precipitation as a function of planetary-boundary-layer moisture convergence forcing model over (a) the forest (wet profile) and (b) the grass (dry profile). Daily amplitude of forcing ranges from 0 to 20 mm day^{-1} (fine dashed to solid line, respectively).

smaller because of initialization with a significantly drier profile. This is quantitatively demonstrated by the β parameter (Table 1): the conversion of moisture convergence to precipitation, $(1 - \beta)$, is a more efficient process in the wetter column, being calculated as 53% and 38% over the wetter and drier initial profile respectively.

Total modelled convective and large-scale precipitation are plotted in Fig. 10, against the maximum daily amplitude of moisture convergence, Q_{max}. For the two cases, a proportionality is observed with respect to convergence rate for both the convective and large-scale precipitation. For a short time integration this result was expected. Although the proportionality is constrained by the linear β factor used here, the initially wetter column tends systematically to produce more precipitation. Nonetheless, for longer simulation periods, the non precipitated moisture probably continues to moisten the column until the calculated averaged precipitation approaches the convergence rate. A nonlinear approach could alter this result. Clearly, despite the two different vegetation types, the influence of the surface is small, and the amount of moisture in the initial profiles accounts for most of these effects.

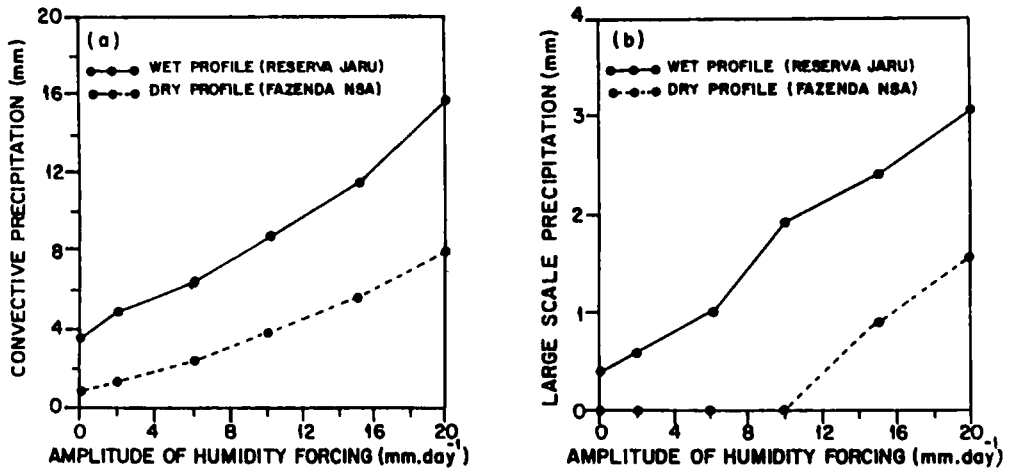

Figure 10. (a) Convective and (b) large-scale precipitation calculated by the SiB-1D model during a 52-hour simulation as a function of the daily planetary-boundary-layer moisture convergence forcing and the profile: wet profile over the forest site and a dry profile over the grass site.

Figure 11 shows the average diurnal cycle of observed precipitation for the ABRACOS sites of Manaus and Ji-Paraná, subdivided into wet- and dry-season data. The dry-season averages represent the four months centred around the driest months of the year at each site, and the wet season averages are for the remaining eight months. Hourly mean precipitation was calculated for Ji-Paraná (1 October 1991 to 12 November 1993 for the Reserva Jarú and Fazenda NSA sites) and for Manaus (2 October 1990 to 31 July 1993 for the Reserva Ducke and Fazenda Dimona sites). All cases have the rainfall maximum at 1530 h local time, exceptionally the Ji-Paraná dry season, which has a mean maximum rainfall at 1330 h local time. A similar observation of the afternoon maxima was obtained by Lloyd (1990) at Reserva Ducke over the period from 1983 to 1985. Consequently, neither the geographical location nor the severity of the dry season have greatly influenced the timing of the daily cycle of convection. Given the limitations imposed by the length of integration and the assumptions within the convective scheme, the observed rainfall is not closely comparable with the calculated precipitation. Nevertheless, it strongly illustrates the dominance of the diurnal processes.

(*e*) *Sensitivity of calculated precipitation to vegetation and soil moisture*

In vegetated areas soil moisture is linked to precipitation through the control of evapotranspiration. Vegetation type and soil type influence the extraction of available soil moisture and the rate of release into the atmosphere through turbulent moisture diffusion into the PBL. Section 4(d) described how wet- and dry-moisture tropospheric profiles affect the calculated precipitation rates within the SiB-1D model. In this section all simulations use the same initial moisture profile, and the influence of forest and grass on precipitation is investigated through a range of soil moisture contents. An initial condition was taken from an observed profile during ABLE-2A over Reserva Ducke, Manaus. Precipitable water for this sounding is the highest among all those used in this work, and equals 52 mm (see Table 1). Three types of vegetation were considered:

(i) the forest of Reserva Ducke (see Sellers *et al.* 1989), referred to as case e1;
(ii) the M2 grass calibrated data set of Fazenda Dimona, referred to as case e2; and
(iii) the M5 grass data set calibrated for Fazenda NSA, referred to as case e3.

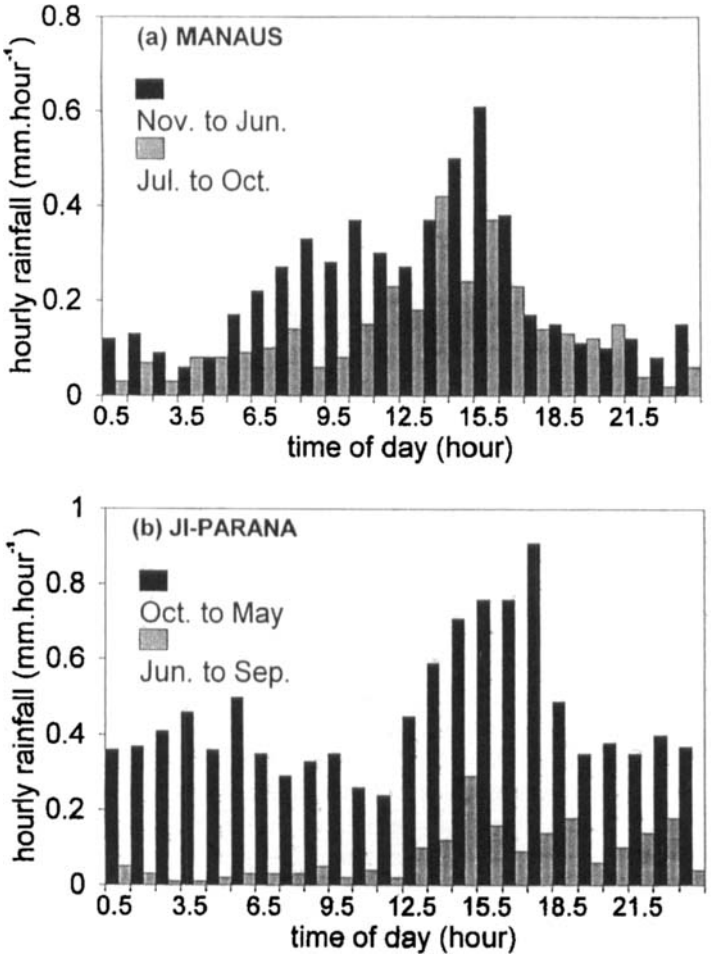

Figure 11. Observed average diurnal cycle of rainfall at the ABRACOS sites of: (a) Manaus for the wet period November to June and dry period July to October, and (b) Ji-Paraná for the wet period October to May and dry period June to September.

All simulations started at 00 UTC 31 July 1985. The geographical coordinates were those for Reserva Ducke and integrations were carried out for 52 hours. The initial and boundary conditions are summarized in Table 1. For each case the fraction of available soil moisture was varied by changing the initial values of soil wetness in the SiB model from 10% to 100%. The available soil moisture, SM_{av}, was calculated as

$$SM_{av} = \frac{(W_r - W_2)}{(W_1 - W_2)} \times 100\% \tag{6}$$

where

$$W_r = \sum_{\text{surface}}^{\text{root}} \frac{(\psi_s/\psi_i) D_i}{z_d}$$

and W_r is the wetness at the rooting layer, W_1 and W_2 are the correspondent wetness at ψ_1 and ψ_2, the water potentials at which the stomata start to open and are completely closed, respectively; ψ_s is the matrix potential at saturation; ψ_i is the matrix potential at level i;

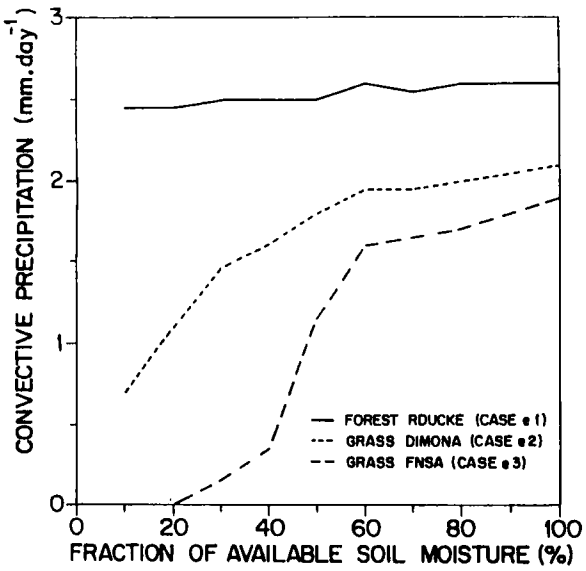

Figure 12. Convective precipitation calculated by the SiB-1D model during a 52-hour simulation as a function of the fraction of available soil moisture for the cases: e1, forest site at Reserva Ducke; e2, grass site at Fazenda Dimona during mission 2 and e3, grass site at Fazenda NSA during mission 5 (see text).

D_i is the depth of the ith layer from the surface up to the root zone; and z_d the total root depth.

Convective precipitation calculated in the 52 hours of simulations is shown in Fig. 12 for different values of initial available soil moisture. We have omitted the large-scale precipitation as convective precipitation accounts for most of the calculated precipitation. The solid curve shows that rainfall over the forest is relatively insensitive to changes in soil moisture. This is a consequence of the evaporation rates over the forest vegetation not being greatly affected by soil potential stress in the drier cases: a result first shown for Manaus by Wright *et al.* (1992). Calculated rainfall over both grassy sites is much smaller than over the forest and appears to be strongly reduced for soil moisture values lower than 60%. Below this value, rainfall for Fazenda NSA declines rapidly, reaching zero at 20% soil moisture: Fazenda Dimona appears to be almost as sensitive. It should be noted that the parameters used for Fazenda NSA for M5 are representative of a time when less energy was partitioned to transpiration than at Fazenda Dimona for M2. As the convective parametrization is forced by local evaporation, it can be seen in Fig. 13 that the evaporation in the three cases is mainly responsible for maintaining the precipitation over the forest and reducing it over the grassy sites.

It is likely that soil moisture under Amazonian vegetation does not reach values as low as 10% of available soil moisture, especially considering the unchanged pattern of observed precipitation over the basin. There remains a question whether forest species are really able to maintain evapotranspiration under such intense soil moisture stress. Also, the soil physical properties assigned to the forest may be more typical of a coarser soil than those present in the area. At high soil moisture contents, these properties seem to reproduce the hydrological behaviour of the soil profile fairly well, probably because the forest soils have a well developed blocky structure. It is not known how these soils behave at low moisture content. Nevertheless, the result to emphasize is that the forest evaporation and its local rainfall do not undergo the 'dry down' behaviour shown for the grassy sites when the available soil moisture drops below 50%.

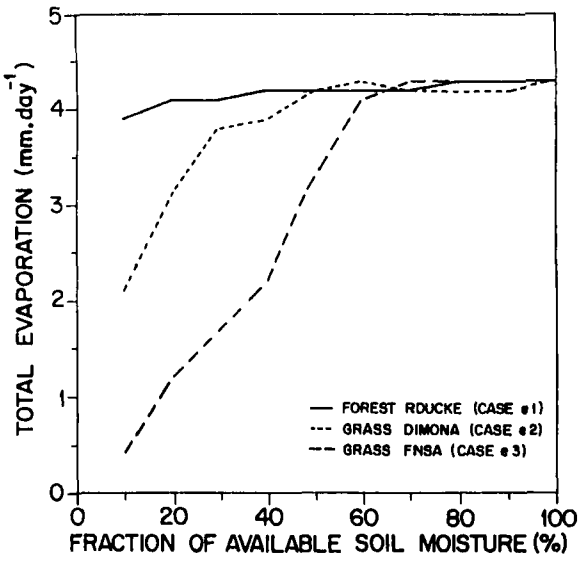

Figure 13. Total evapotranspiration calculated by the SiB-1D model during a 52-hour simulation as a function of the fraction of available soil moisture for the cases: e1, forest site at Reserva Ducke; e2, grass site at Fazenda Dimona during mission 2; and e3, grass site at Fazenda NSA during mission 5 (see text).

5. Concluding remarks

High deforestation rates in Amazonia over the last two decades have raised the question as to how climate, and particularly precipitation, might be affected as primary forest is replaced by pasture. Convection is a major mechanism generating rainfall in the Tropics and strongly depends on low-level moisture convergence to trigger cloud formation and precipitation. Delving further, the convective processes are closely linked to the surface-energy balance, as surface evaporation is a source of water vapour to the PBL and ultimately to the base of the convective clouds. For the Amazonia, it has been shown that ranchland pasture has less net radiation and is very sensitive to soil water stress during the dry season, leading to a different partitioning of surface energy. When the fraction of available soil moisture falls below 60%, the uptake of water by the pasture is impeded by the low water potential in the shallow root system.

A one-dimensional atmospheric physical model, SiB-1D, was developed and constructed by coupling the SiB surface model with a model of the atmospheric column, retaining the physical processes of the COLA GCM. In this way it has been possible to simulate how these processes interact over short time-scales (days) when the large-scale flow is assumed to be weak. The SiB model was calibrated for two grassy vegetation types in Amazonia: Fazenda Dimona near Manaus, Central Amazonia, during the early dry season; and Fazenda Nossa Senhora Aparecida, near Ji-Paraná, south-west Amazonia, during the mid dry season. The latter set of parameters represented a more stressed vegetation as compared with the former. Model parameters were derived wherever possible from *in situ* measurements and those remaining were evaluated using an iterative optimization procedure. The calibrated SiB-1D model was then used to simulate the surface-energy balance and boundary-layer evolution over either the forest or the grass site. The calculations were compared with observations from the RBLE and ABRACOS and a reasonable agreement was found for the 48-hour simulations.

Sensitivity tests of the Kuo convective parametrization were carried out using a range of external PBL moisture convergences as likely representations of actual low-level convergence. Even by setting strongly contrasting initial conditions, a wet and a dry column over the forest and the grass, respectively, the effects on the calculated precipitation were constrained by the convective scheme, suggesting that the surface processes had little or no influence. Table 3 shows that, with only a few exceptions, most GCM simulations have calculated a decrease of evaporation, precipitation and water vapour convergence. Furthermore, the resulting changes in GCM results have occurred basically in the dry season, e.g. the changes of -2.0 mm day^{-1} and -2.4 mm day^{-1} in evaporation and precipitation shown by Nobre *et al.* (1991). As it is well known that massive moisture convergence exists in the Amazon region during the wet season (Salati and Nobre 1991), the results of this 1-D model are well supported, given the prevailing large-scale circulation and moisture inflow into the continent: the precipitation over the region could only slightly be affected by a change in the surface vegetation in these circumstances.

TABLE 3. 'DEFORESTATION' MINUS 'FOREST' CALCULATED DIFFERENCES OF EVAPORATION (ΔE), PRECIPITATION (ΔP), AND MOISTURE CONVERGENCE ($\Delta(P - E)$), FOR SOME PREVIOUS GCM SIMULATIONS

	ΔE	ΔP	$\Delta(P - E)$
	mm day^{-1}		
Lean and Warrilow (1989)	−0.8	−1.3	−0.5
Nobre *et al.* (1991)	−1.3	−1.8	−0.5
Dickinson and Kennedy (1992)	−0.7	−1.4	−0.7
Lean and Rowntree (1993)	−0.5	−0.8	−0.2
Henderson-Sellers *et al.* (1993)	−0.6	−1.6	−1.0
Manzi (1993)	−2.7	+1.1	+3.7
Polcher and Laval (1994)	−0.3	0.0	+0.3

An assessment of the interaction between soil moisture, vegetation and precipitation was accomplished with the SiB-1D model given no moisture convergence over a short-term simulation of 52 hours. For either a forest or a grassy surface, a range of available soil moisture, varying from 10 to 100%, was used for the initial condition. The results show that forest evaporation and the corresponding rainfall appeared to be insensitive to soil water contents. On the other hand, for pasture vegetation, much lower evaporation was generated compared with the forest, as well as a significant sensitivity to the pasture-land vegetation type over soil moisture. Calculated precipitation over the pasture sites declined rapidly below a threshold soil moisture availability of 60%. Observational evidence over the central and southern Amazon shows the presence of a weak large-scale subsidence during most of the southern winter, a phenomenon compatible with zero moisture convergence or, in some cases, moisture divergence. In assuming no convergence in this sensitivity test, the resultant changes in evaporation and precipitation cited by Nobre *et al.* (1991) for the dry season are a useful initial comparison: the change of -2.4 mm day^{-1} in precipitation matches the points at a soil moisture availability of about 60% (Fig. 12), and similarly a change of -2.0 mm day^{-1} in evaporation matches the points around a soil moisture availability of 40% (Fig. 13). It should be noted that the 1-D approach is not fully comparable with 3-D GCM results as the former is not able to represent the nonlinearities inherent in the interactions between the large-scale and the physical processes. However, this result

supports the idea that during dry spells the surface might play a significant role in the post-deforestation climate, an aspect already anticipated by some previous GCM results.

ACKNOWLEDGEMENTS

Our gratitude to those who shared with us their experience in the field campaigns of the ABRACOS and RBLE: M. Hodnett, R. Lyra, E. Rocha, J. Gash, J. Roberts, J. Shuttleworth, A. McWillian, O. Cabral, A. Lola, G. Fisch, A. Culf, H. Bastable, R. Senna, M. Miranda, A. Manzi, P. Regnier, R. Dallarosa, P. R. Carvalho, J. Nogueira, E. Paiva, H. Xavier and E. Lacerda. We acknowledge the support of RBLE-II by the Fundação de Amparo à Pesquisa do Estado de São Paulo under grant no 93/0642-7 and of Conselho Nacional de Pesquisa e Desenvolvimento Tecnológico under grant no 63003-93-9. We also thank P. Silva Dias (Universidade de São Paulo) and E. Souza (Universidade Federal da Paraiba) for contributions on the convection parametrization, Y. Xue, P. Dirmeyer, J. Shukla (COLA) and M. Heiser (University of Maryland). This paper is dedicated to the memory of Prof. Yelisetty Viswanadham. We miss his friendship.

APPENDIX

Site description and calibration procedure

Meteorological data were recorded during M1, M2 and M5 periods (see sections 2 and 3) by an automatic weather station comprising the following variables: incoming shortwave radiation, net radiation, horizontal wind speed, air temperature and humidity, and precipitation. Soil moisture was measured at 0.2 m depth intervals using a neutron probe. Turbulent fluxes were measured from a micrometeorological profile tower for M2, and for M5 using the 'Hydra' eddy correlation device (Institute of Hydrology, UK). For details see Wright *et al.* (1992), Wright *et al.* (1995) and Bastable *et al.* (1993).

The vegetation at Fazenda Dimona was mostly tropical grasses of the variety *Brachiaria decumbens* and *Brachiaria humidicola* (Kikuyo da Amazonia). The dominant soils in the Manaus region, and especially at Fazenda Dimona are clayey Yellow Latosols (Tipic Haplortlox). Hodnett *et al.* (1995) provide a full description of the soil moisture status at the Fazenda Dimona site. Field capacity was estimated from field measurements of available soil moisture: they were shown to be 0.11, 0.84, 0.60, 0.65, 0.72, 0.60 and 0.58 m^3m^{-3}, at depths of 10, 20, 40, 60, 80, 100 and 120 cm, respectively. The fraction of available soil water, as discussed in section 2, refers to the top 1 m and is estimated as the soil water in excess of the wilting point divided by the total soil water between wilting point and field capacity. Wilting point was taken as the matric potential at -15 bar for a clayey Yellow Latosol, equal to 0.25 m^3m^{-3}, and is assumed to be independent of depth (Freitas Jr 1981). The M5 site was predominantly covered by the grass species of *Brachiaria Brizantha* and the soil is a Red-yellow Podzol (Orthoxic Tropohumult).

The SiB model in an off-line mode was used to derive the best parameters representative of the experimental data collected at the grass sites of Fazenda Dimona (Manaus, M2) and Fazenda NSA (Ji-Paraná, M5). In this mode, the SiB model is decoupled from the atmospheric model and forced by the meteorological surface variables. The following rain-free days were chosen for calibration: days 3, 9, 10, 11, 14, 16 and 17 July 1991 from M2 and days 17 to 24 July 1993 from M5. In the calibration exercise undertaken here, a sub-set of parameters was identified which could be evaluated by *in situ* measurements and eliminated from the optimization procedure. The calibration can then minimize the difference between simulated surface fluxes and values by optimizing only those

TABLE A.1. RESULTS OF SIMULATIONS USING INITIAL AND OPTIMIZED SETS OF PARAMETERS. COLUMN I REFERS TO THE INITIAL SET (NOBRE *et al.* 1991); COLUMNS II AND III SHOW THE OPTIMIZED SET OF PARAMETERS AT FAZENDA DIMONA (M2) AND FAZENDA NSA (M5), RESPECTIVELY (SEE TEXT).

Parameter	I	II	III
Porosity (θ_s) (m^3m^{-3})	0.42	0.53	0.46
Saturated hydraulic conductivity (K_s) ($m\ s^{-1}$)	2×10^{-6}	1×10^{-5}	1×10^{-5}
Fractional area covered by canopy store layer (V_c)	0.80	0.84	0.79
Leaf-area index of the canopy store layer (L_{tc}) (m^2m^{-2})	2.15	1.22	1.61
Roughness length (z_0) (m)	0.076	0.026	0.022
Zero-plane displacement (d) (m)	0.26	0.17	0.70
Fractional area of ground cover vegetation (V_{gs})	0.85	0.59	0.89
Leaf-area index of the ground cover vegetation (L_{tgs}) (m^2m^{-2})	2.40	1.03	0.43
Green-leaf fraction of canopy cover (N_c)	0.95	0.99	0.93
Light-dependent stomatal response parameters:			
(a) ($J\ m^{-3}$)	11 312	6000	11 554
(b) ($W\ m^{-2}$)	1.0	1.6	2.1
(c) ($s\ m^{-1}$)	110.7	95.2	110.0
Stomatal response factor to water vapour deficit (h_6) (hPa^{-1})	0.0191	0.0200	0.0184
Leaf-water-potential parameters:			
(ψ_1) (m)	−30	−15	−26
(ψ_2) (m)	−230	−409	−224
Root resistance per unit length (R) ($s\ m^{-1}$)	10 000	10 992	7434
Root-mean-square deviation	491	160	—
	322	—	235

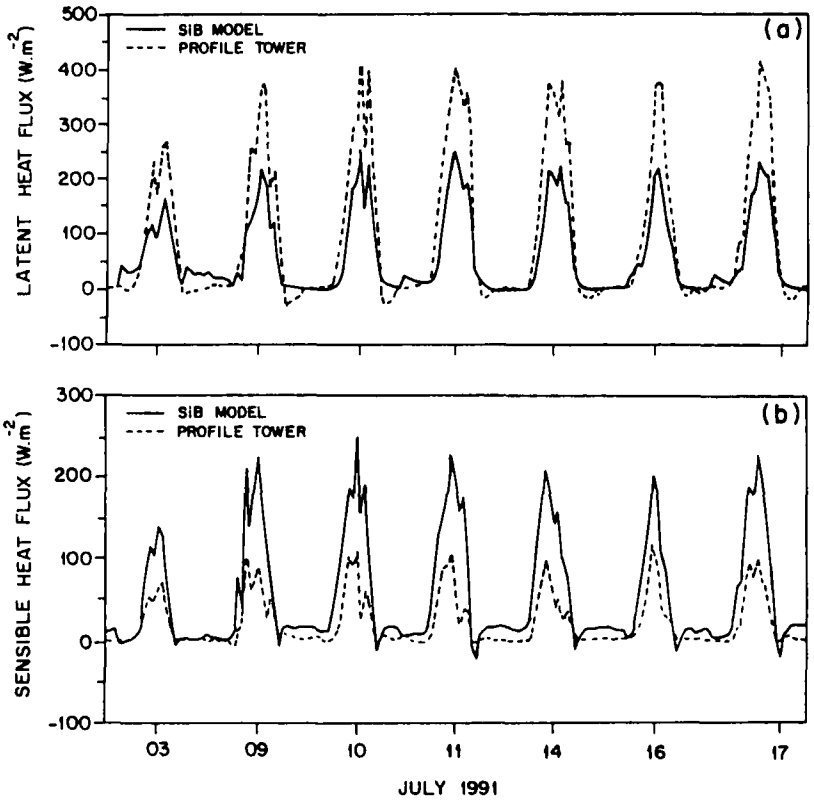

Figure A.1. Surface turbulent energy fluxes over Fazenda Dimona during mission 2 as measured by profile tower and calculated by the SiB model using the initial set of parameters: (a) latent-heat flux, and (b) sensible-heat flux.

parameters which have the most uncertainty or have no associated field measurement. For the optimization procedure, an initial set of parameters representing degraded pasture was taken from Nobre *et al.* (1991), and since Sellers *et al.* (1989) have thoroughly described the iterative optimization method, we simply summarize the main steps as follows:

(i) parameters measured *in situ* replace the initial input data set, and the SiB model is run using the near-surface meteorological data as forcing variables to calculate the surface fluxes;
(ii) an assessment of the quality of the simulation is given by the difference between the calculated and the observed evaporative fraction (latent-heat flux divided by the sum of latent- plus sensible-heat flux), weighted by the absolute value of the observed latent-heat flux;
(iii) the deviations for each time step are used to calculate the mean deviation error and input to a least-squares minimization algorithm, ZXSSQ (IMSL 1984), to determine numerically the partial derivatives of each deviation with respect to the optimized parameters. The procedure is repeated until the best set of parameters is found, that is until each deviation cannot be reduced further.

Prognostic variables of the model were initialized as field data. The storage of intercepted water was set to zero, and the temperatures of the canopy and ground cover were set equal to the temperature measured at the reference height. Initial values of soil wetness

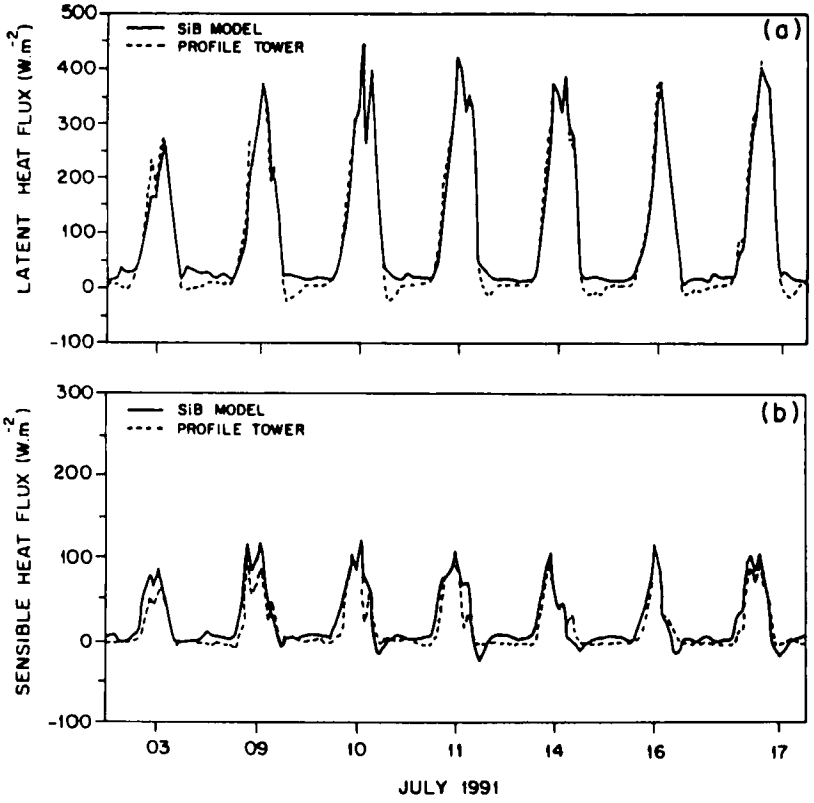

Figure A.2. As Fig. A.1 but using the optimized set of parameters.

were interpolated from field data to provide the values of surface, root and recharge layer wetness W_1, W_2 and W_3, respectively: 0.70, 0.76 and 0.90 respectively for M2, and 0.42, 0.67 and 0.67 for M5.

Table A.1 summarizes the values of the initial and optimized parameters. Porosity, θ_s, and saturated hydraulic conductivity, K_s, were based on *in situ* measurements and on measurements in similar soils (Freitas Jr 1981; Correa 1984). Values of the fractional area covered by canopy store layer, V_c, roughness length, z_0, and zero-plane displacement, d, are from analysis of aerodynamic profiles derived by Wright *et al.* (1992) and Wright (personal communication). McWilliams (personal communication) provided the values of leaf-area index of the canopy store layer, L_{tc}, collected during M2 and M5. The remaining parameters shown in Table A.1 involve more uncertainty in their specification, thus were altered in the optimization routine until a 'best fit' was accomplished.

The root-mean-square deviation between the observed and calculated turbulent fluxes is also shown in Table A.1 to illustrate the quality of the simulation. The observed and calculated fluxes, using the initial and optimized set of parameters for M2, are shown in Figs. A.1 and A.2, respectively. These results show that the initial set overestimated the sensible-heat flux, thus underestimating evapotranspiration, while the optimized set considerably improved the estimation and fitted the observed fluxes with satisfactory agreement. For M5, shown in Figs. A.3 and A.4, there are improvements when the initial set is compared with the optimized one, although the agreement is not as good as for M2.

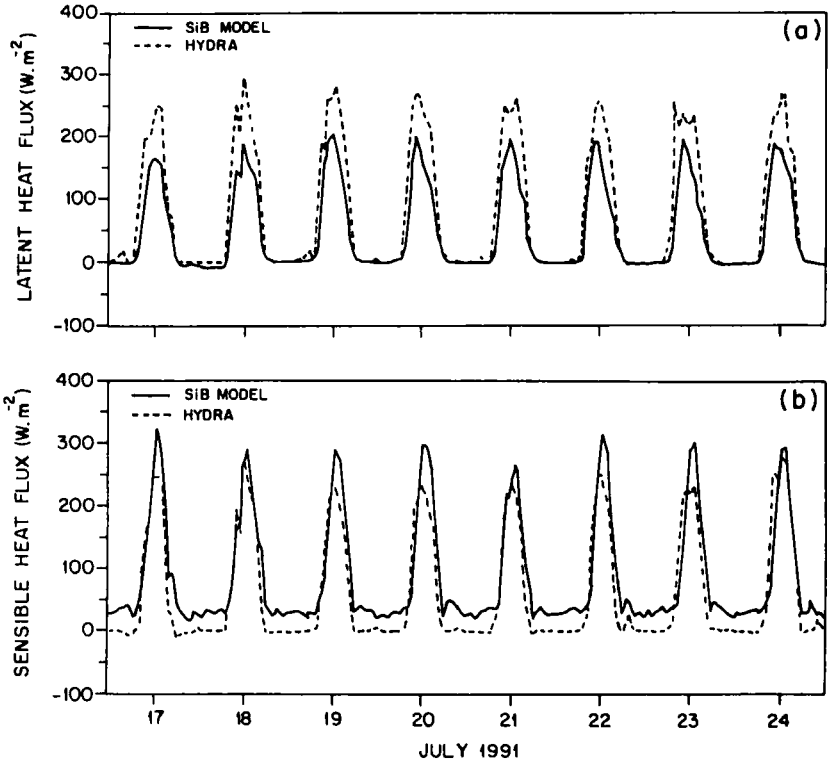

Figure A.3. Surface turbulent energy fluxes over Fazenda NSA during mission 5 (see text) as measured by the Hydra eddy-correlation device and calculated by the SiB model using the initial set of parameters: (a) latent-heat flux, and (b) sensible-heat flux.

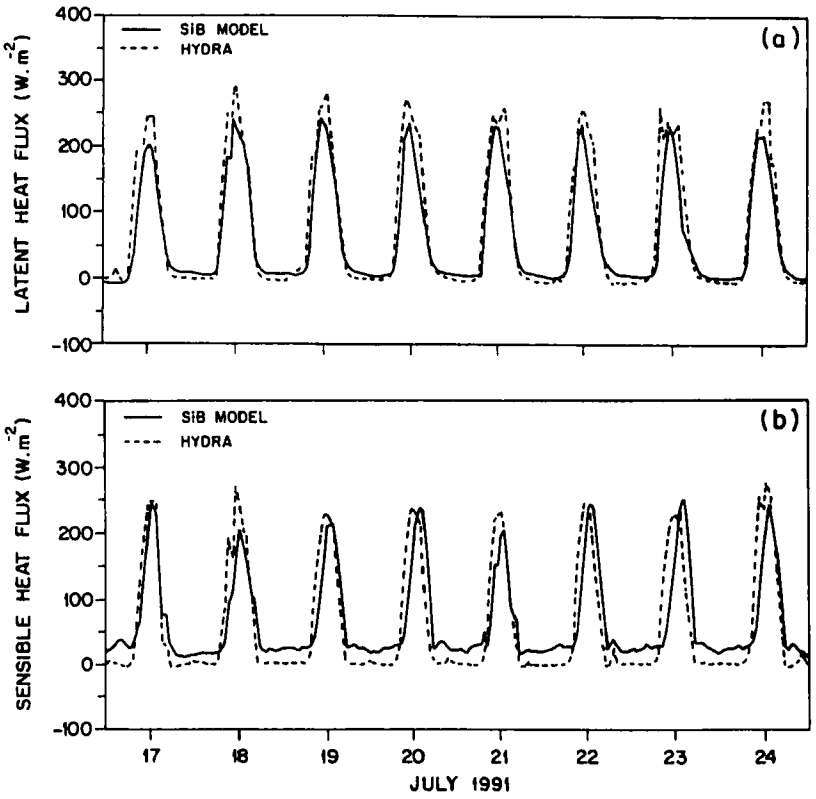

Figure A.4. As Fig. A.3 but using the calibrated set of parameters.

It was noticed that in M5 the sensible-heat flux was slightly out of phase as compared with observations, while the daytime peaks of calculated latent-heat flux rarely reached the observed ones. Even considering the M5 calibration to be quite reasonable, an attempt was made to explain this discrepancy by checking the source of observed data: during M2 the field data were mostly derived from a profile of psychrometers and anemometers mounted vertically on a 9 m tower, and the average hourly flux was calculated using the Bowen-ratio method, since net radiation and soil heat flux were available. The direct consequence of using this method is that it exactly closes the surface-energy balance, and since the SiB model flux calculations must close the energy balance there is an implicit level of agreement. On the other hand, the observed flux used here for M5 was measured using the Hydra eddy-correlation device. Although this instrumentation has been used successfully in Amazonia and provided experimental data for other calibrations (Sellers *et al.* 1989; Wright *et al.* 1995), use of the Hydra does not guarantee closure of the energy balance and may account for some of the discrepancy for the M5 comparison.

References

Anthes, R. A. 1977 Hurricane model experiments with a new cumulus parameterization scheme. *Mon. Weather Rev.*, **105**, 270–286

1984 Enhancement of convective precipitation by mesoscale variations in vegetative covering in semiarid regions. *J. Clim. Appl. Meteorol.*, **23**, 541–554

Bastable, H. G., Shuttleworth, W. J., Dallarosa, R. L. G., Fisch, G. and Nobre, C. A. 1993 Observations of climate, surface radiation and albedo over cleared and undisturbed Amazonian forest. *Int. J. Climatol.*, **13**, 783–796

Cerri, C. C. and Volkof, B. 1987 Carbon content in a yellow latosol of central Amazon rainforest. *Acta Oecologica*, **8**, 29–42

Corrêa, J. C. 1984 Características físico-hídricas do latossolo amarelo, podzólico vermelho-amarelo e podzol hidromórfico no estado do Amazonas. *Pesquisa Agropecuária Brasileira*, **19**, (3), 347–360

Davies, R. 1982 'Documentation of the solar radiation parametrization in the GLAS climate model'. NASA Tech. Memo 83961

Dickinson, R. E. and Henderson-Sellers, A. 1988 Modelling tropical deforestation: A study of GCM land-surface parametrization. *Q. J. R. Meteorol. Soc.*, **114**, 439–462

Dickinson, R. E. and Kennedy, P. 1992 Impacts on regional climate of Amazon deforestation. *Geophys. Res. Lett.*, **19**, 1947–1950

Freitas Jr, E. de 1981 'Retenção e disponibilidade de água em dois solos da Amazônia Central'. Dissertação de Mestrado. Escola Superior de Agricultura Luiz de Queiroz, da Universidade de São Paulo, USP-Piracicaba, SP

Harshvardhan, T. and Corsetti, T. G. 1984 'Longwave radiation parameterization for the UCLA/GLAS GCM'. Technical memorandum 86072. Greenbelt, NASA, MD

Harshvardhan, T., Davies, R., Randall, D. A. and Corsetti, T. G. 1987 A fast radiation parameterization for the general circulation models. *J. Geophys. Res.*, **92**, 1009–1016

Henderson-Sellers, A., Dickinson, R. E., Durbridge, T. B., Kennedy, P. J., McGuffie, K. and Pitman, A. J. 1993 Tropical deforestation: Modelling local to regional-scale climate change. *J. Geophys. Res.*, **98**, 7289–7315

Hodnett, M. G., da Silva, L. P., da Rocha, H. R. and Senna, R. C. 1995 Seasonal soil water storage changes beneath central Amazonian rainforest and pasture. *J. Hydrol.*, **170**, 233–254

IMSL (International Mathematical and Statistical Library) 1984 Chapter Z. IMSL, ZXSSQ-1 to ZXSSQ-7

Kuo, H. L. 1974 Further studies of the parameterization of the interactions of cumulus convection on large-scale flow. *J. Atmos. Sci.*, **31**, 1232–1240

Lacis, A. A. and Hansen, J. E. 1974 A parameterization for the absorption of solar radiation in the earth's atmosphere. *J. Atmos. Sci.*, **31**, (1), 118–133

Lean, J. and Rowntree, P. R. 1993 A GCM simulation of the impact of Amazonian deforestation on climate using an improved canopy representation. *Q. J. R. Meteorol. Soc.*, **119**, 509–530

Lean, J. and Warrilow, D. A. 1989 Climate impact of Amazonian deforestation. *Nature*, **342**, 311–313

Lloyd, C. R. 1990 The temporal distribution of Amazonian rainfall and its implication for forest interception. *Q. J. R. Meteorol. Soc.*, **116**, 1487–1494

Manzi, A. O. 1993 'Introducion d'un schéma des tranferts sol-vegétation-atmosphère dans un modèle de circulation générale et application à la simulation de la deforestation Amazonienne'. PhD Thesis, Paul Sabatier University, Toulouse, France

Martin, C. L., Fitzjarrald, D., Garstang, M., Oliveira, A. P., Greco, S. and Browell, E. 1988 Structure and growth of the mixing layer over the Amazonian rain forest. *J. Geophys. Res.*, **93**, (D2), 1361–1375

Mellor, G. L. and Yamada, T. 1982 Development of a turbulence closure model for geophysical fluid problems. *Rev. Geophys. Space Phys.*, **20**, (D4), 851–875

Nobre, C. A., Sellers, P. J. and Shukla, J. 1991 Amazonian deforestation and regional climate change. *J. Climate*, **4**, 957–987

Pereira, M. da C. and Setzer, A. W. 1989 'Detecção de queimadas e plumas de fumaça na Amazônia através de imagem de satélite NOAA'. PI(INPE-3924-PRE/958)

Philips, N. 1979 'The nested grid model'. NOAA Tech. Rep. NWS-22

Pielke, R. A., Dalu, G. A., Snook, J. S., Lee, T. J. and Kittel, T. G. F. 1991 Nonlinear influence of mesoscale land use on weather and climate. *J. Climate*, **4**, 1053–1069

Polcher, J. and Laval, K. 1994 The impact of African and Amazonian deforestation on climate change. *J. Hydrol.*, **153**, (3–4), 389–406

Rabin, R. M., Stadler, S., Wetzel, P. J., Stensrud, D. J. and Gregory, M.	1990	Observed effects of landscape variability on convective clouds. *Bull. Am. Meteorol. Soc.*, **71,** (3), 272–280
Roberts, J. M., Cabral, O. M. R. and de Aguiar, L. F. F.	1990	Stomatal and boundary-layer conductances in an Amazonian *terra firme* rain forest. *J. Appl. Ecol.*, **27,** 336–353
Rocha, H. R. da, Nobre, C. A. and Barros, M. C.	1989	Variabilidade natural de longo prazo do ciclo hidrológico da Amazônia. *Climanálise*, **4(12),** 31–35
Salati, E. and Nobre, C. A.	1991	Possible climatic impacts of tropical deforestation. *Clim. Change*, **19,** 177–196
Sato, N., Sellers, P. J., Randall, D. A., Schneider, E. K., Shukla, J., Kinter III, J. L., Hou, Y. T. and Albertazzi, E.	1989	Effects of implementing the Simple Biosphere Model in a general circulation model. *J. Atmos. Sci.*, **46,** (18), 2757–2782
Schadler, G.	1990	Triggering of atmospheric circulations by moisture inhomogeneities of the earth's surface. *Boundary-Layer Meteorol.*, **51,** 1–30
Sellers, P. J., Mintz, Y., Sud, Y. C. and Dalcher, A.	1986	A Simple Biosphere Model (SiB) for use within general circulation models. *J. Atmos. Sci.*, **43,** (6), 505–531
Sellers, P. J., Shuttleworth, W. J., Dorman, J. L., Dalcher, A. and Roberts, J. M.	1989	Calibrating the Simple Biosphere Model for Amazonian tropical forest using field and remote sensing data. Part I: Average calibration with field data. *J. Appl. Meteorol.*, **28,** (8), 727–759
Shuttleworth, W. J.	1988	Evaporation from Amazonian rain forest. *Proc. R. Soc. London* **B233,** 321–346
Silva Dias, P. L., Bonatti, J. P. and Kousky, V. E.	1987	Diurnally forced tropical tropospheric circulation over South America. *Mon. Weather Rev.*, **115,** (8), 1465–1478
Slingo, J. M.	1987	The development and verification of a cloud prediction scheme for the ECMWF model. *Q. J. R. Meteorol. Soc.*, **113,** 899–927
Tiedtke, M.	1984	The effect of penetrative cumulus convection on the large-scale flow in a general circulation model. *Beitr. Phys. Atmos.*, **57,** (2), 216–239
Wright, I. R., Gash, J. H. C., da Rocha, H. R., Shuttleworth, W. J., Nobre, C. A., Maitelli, G. T., Zamparoni, C. A. G. P. and Carvalho, P. R. A.	1992	Dry season micrometeorology of central Amazonian ranchland. *Q. J. R. Meteorol. Soc.*, **118,** 1083–1099
Wright, I. R., Manzi, A. O. and da Rocha, H. R.	1995	Surface conductance of Amazonian pasture: model application and calibration for canopy climate. *Agric. For. Meteorol.*, **75,** (1–3), 51–70
Xue, Y., Sellers, P. J., Kinter, J. K. and Shukla, J.	1991	A Simplified Biosphere Model for global climate studies. *J. Climate*, **4,** (3), 345–364